Adaptation of flipper-mud interactions enables effective terrestrial locomotion on muddy substrates

Shipeng Liu[1], Boyuan Huang[1] and Feifei Qian[*,1]

***Abstract*—Moving on natural muddy terrains, where soil composition and water content vary significantly, is complex and challenging. To understand how mud properties and robot-mud interaction strategies affect locomotion performance on mud, we study the terrestrial locomotion of a mudskipper-inspired robot on synthetic mud with precisely-controlled ratios of sand, clay, and water. We observed a non-monotonic dependence of the robot speed on mud water content. Robot speed was the largest on mud with intermediate levels of water content (25%-26%), but decreased significantly on higher or lower water content. Measurements of mud reaction force revealed two distinct failure mechanisms. At high water content, the reduced mud shear strength led to a large slippage of robot appendages and a significantly reduced step length. At low water content, the increased mud suction force caused appendage entrapment, resulting in a large negative displacement in the robot body during the swing phase. A simple model successfully captured the observed robot performance, and informed adaptation strategies that increased robot speed by more than 200%. Our study is a beginning step to extend robot mobility beyond simple substrates towards a wider range of complex, heterogeneous terrains.**

***Index Terms*—Biologically-Inspired Robots; Legged Robots; Contact Modeling**

I. Introduction

MUDDY substrates exist widely in natural environments. Capabilities to effectively move across different muddy surfaces can empower terrestrial robots for a variety of critical missions, such as nearshore exploration, autonomous delivery, and search and rescue after landslides. Moving on mud can be extremely challenging [1]–[4]. The strength and rheology of mud can exhibit significant variations due to subtle changes in parameters such as grain size, organic matter, and water content [5]–[7]. Misapplied interaction strategies could result in catastrophic failures of robot locomotion in mud, including sinkage, slippage, or even complete entrapment.

Due to the complex rheology and heterogeneous nature of these natural deformable terrains, most robot locomotion studies and control methods were focused on rigid ground [8]–[10]. Recent research began to explore principles of robot locomotion performance on dry, homogeneous granular media [4], [11]–[15]. It was discovered that for yield-stress [16] substrates like sand and mud, robot locomotor performance (e.g., speed) depended sensitively on the interaction strategies between robot appendages and substrates [11], [13], [14]. Sand and mud behave solid-like when external forcing is below the critical yield stress, but can flow like a fluid when the yield stress is exceeded [17], [18]. By adapting the design [13], [14] or the motion [11], [12], [15] of appendages, robots could effectively solidify [11], [13], [14] or fluidize [12] the granular substrates to achieve agile locomotion on a wide variety of dry, granular terrains.

The key challenge in creating the next-generation mobile robots with capabilities to robustly cope with natural terrains is expanding these principles from dry, homogeneous granular media to wet [19], heterogeneous substrates like mud. Natural muddy terrains are often comprised of particles with sizes spanning orders of magnitude — from clay particles up to a few microns to sand particles up to a few millimeters — as well as a wide range of water content. Unlike dry sand particles that interact with each other through repelling forces, with the presence of water the fine clay can produce attracting forces between particles, introducing significant changes to mud rheology, such as cohesion [20]. As a result, mud can exhibit a variety of mechanical behaviors, from gel-like fluid to compliant solids, upon robot appendage interactions. While there was a large body of studies on mud rheological behaviors [5], [6], [21]–[23], most existing studies were focused on mud suspensions, while the mechanical behaviors of mud that were most relevant to terrestrial robot locomotion (*i.e.,* close to jamming phase [7], [24]) were relatively unexplored. In most recent studies, researchers have begun to investigate the mud rheology close to the near-jamming range [7], [24]. However, these studies were largely focused on earth sciences questions. The relationship between mud rheological responses and robot locomotion performance [25]–[27] was much less understood.

To begin to understand how mud properties influence robot locomotion performance, we investigate the locomotion of a mudskipper-inspired robot [13], [15] on mud mixtures with precisely controlled clay-to-sand ratio and systematically varied water content. Sec. II describes the robot and our experiment setup. In Sec. III, we discuss the observed robot speed on mud mixtures with different water content. We find that the robot can move effectively on mud mixtures with intermediate water content (25%-26%), but exhibits significant locomotion failure with only a few percent of water content variation. To reveal the failure mechanisms, we empirically measure the mud resistive forces during horizontal and vertical

Manuscript received: May, 2nd, 2023; Revised July, 17th, 2023; Accepted September, 20th, 2023.

This paper was recommended for publication by Editor Abderrahmane Kheddar, upon evaluation of the Associate Editor and Reviewers' comments. This research was supported by funding from the National Science Foundation (NSF) CAREER award #2240075, and the NASA Planetary Science and Technology Through Analog Research (PSTAR) program, Award # 80NSSC22K1313.

[1]Shipeng Liu, Boyuan Huang and Feifei Qian are with Department of Electrical and Computer Engineering, University of Southern California, Los Angeles, CA, USA. shipengl@usc.edu; boyuanhu@usc.edu; feifeiqi@usc.edu (*corresponding author: Feifei Qian*)

Digital Object Identifier (DOI): see top of this page.

motion of robot appendages, and create a simple model to explain the observed dependence of robot performance on water content. The model captures the experimentally observed robot performance and predicts adaptations of robot flipper motion to mitigate the observed failure. In Sec. IV we implement the adapted strategies in experiments and show that the model-predicted locomotor strategies can significantly improve the robot speed on previously-failing mud mixtures.

II. Materials and Methods

A. Robot

To investigate how locomotion performance in mud was affected by mud properties and flipper motions, we developed a bio-inspired robot as a robophysical [28] model to perform controlled laboratory experiments. The robot was inspired by the mudskipper (*Periophthalmus barbarus* [29] (Fig. 1A), a small fish that can use its pectoral fins to produce effective locomotion on mud surfaces through a "crutching" motion. The high mobility of mudskippers has inspired the development of flipper-based robots with significantly improved capabilities to move on cohesionless dry sand [13], [15]. Here we seek to use the mudskipper-inspired platform to test hypotheses for cohesive substrates, and extend the principles of flipper-based locomotion to a broader range of soft, yielding terrains.

Modeled after the mudskipper's pectoral fins, two flipper arms (PLA plastic) were attached on the front side of the robot body (Fig. 1B) to produce flipper-driven locomotion on mud. Each flipper arm was actuated with two motors: a servo motor (FeeTech FS5115M) that controls the vertical adduction angle, β, and a brushless motor (T-Motor R60) that controls the horizontal sweeping angle, α (Fig. 1C). The length of each flipper arm was 12 cm, measured between the center of the sweeping motor and the center of the flipper, with a rectangle-shaped (3 cm $\times$ 5 cm) flipper at the distal end of the arm to provide thrust in mud. A 1.5 cm $\times$ 1.5 cm rectangular-shaped extrusion was designed below the bottom of the robot to create drag on the robot body during locomotion. The angular positions of the sweeping and adduction motors were commanded by a single-board computer (Raspberry Pi), and controlled by two motor controllers (ODrive v3.6 and Adafruit Servo Bonnet, respectively).

B. Flipper kinematics

A symmetric "crutching" gait was used in this study, where both limbs performed the same kinematics during each gait cycle. A gait cycle includes the following four phases:

1) Flipper insertion phase, where α was kept constant at $-\frac{\pi}{6}$ radians, as β increased from 0 radians to $\frac{5\pi}{18}$ radians.
2) Flipper sweeping phase, where β was kept constant at $\frac{5\pi}{18}$ radians, as α increased from $-\frac{\pi}{6}$ radians to $\frac{\pi}{6}$ radians.
3) Flipper extraction phase, where α was kept constant at $\frac{\pi}{6}$ radians, as β decreased from $\frac{5\pi}{18}$ radians to 0 radians.
4) Flipper swing phase, where β was kept constant at 0 radians, as α decreased from $\frac{\pi}{6}$ radians to $-\frac{\pi}{6}$ radians.

The sweeping and adduction angular velocities, ω_α and ω_β, were both kept at 4.2 rad/s for all experiment trails except the adaptation experiments in Sec. IV. Both angular velocities were chosen to be larger than the inertial effect threshold [30] to allow investigating the effect of both hydro-static and hydro-dynamic like forces [12]. In all trials, the maximal flipper insertion depth was kept at 3.5 cm, at which the robot exhibited a rich set of mud interaction behaviors and failure modes.

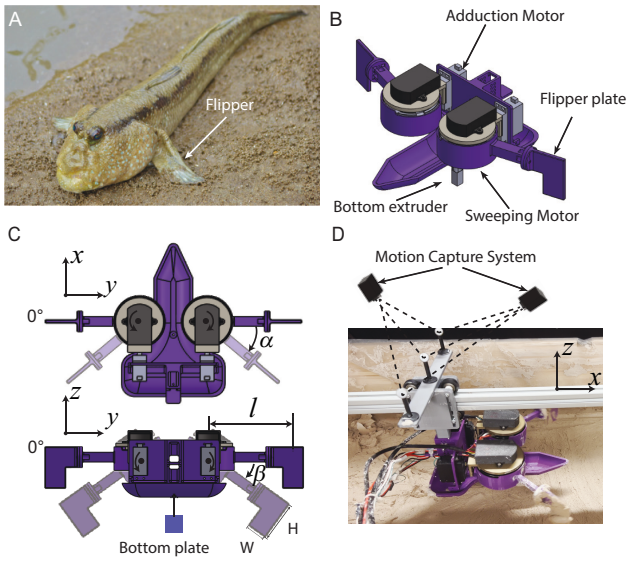

Fig. 1. Laboratory experiments to study locomotion on mud. (A) Mudskipper, the biological locomotor that the robot was modeled from. Photo credit Wikimedia Commons. (B) A mudskipper-inspired robot as a physical model of the mudskipper, to systematically test the effect of flipper motion on robot locomotion performance on mud. (C) Each flipper arm has two degree of freedom (DoF): a sweeping angle, α, and an adduction angle, β. The flipper arm length, l, is 12 cm. The width and height of the flipper are W = 3 cm and H = 5 cm. D) Apparatus to test robot locomotion performance on mud. Two motion capture cameras were used to track the robot's fore-aft position, while a supporting rail was employed to precisely control the flipper insertion depth.

C. Experiment Setup

Robot locomotion experiments were performed in a 125 cm $\times$ 65 cm $\times$ 17 cm trackway (Fig. 1D). We created synthetic mud mixtures by fully mixing a controlled volume of sand (Gilson, 150 $\sim$ 600 μm particle diameter silica), clay (Seattle Pottery Supply, Edgar Plastic Kaolin), and water. These synthetic mud behaves rheologically similar to natural mud [5], [7], and allows for systematic variation of mud properties. By adjusting the ratio of the ingredients (e.g., clay-to-sand ratio, and water content), the rheological properties of mud can be varied over a wide range for locomotion tests. For data reported in this study, the clay-to-sand ratio was kept as 3:1, whereas the water content, W, was systematically varied between 24% and 32%, with 24% being close to the lower limit where below which the mud could not be evenly mixed across the trackway, and 32% being close to the upper limit where beyond which the mud strength was too low that the robot could not generate effective forward motion. Here the water content is defined as $W = V_w/(V_w + V_c + V_s)$, where V_w represents the volume of water, V_c represents the volume of clay, and V_s represents the volume of sand. Both V_c and V_s are occupied volumes (*i.e.,* includes both solid volume and air

space before mixing). 3 locomotion trials were performed for each water content. The surface layer of the mud substrate was re-mixed and leveled manually between trials to eliminate the effect of disturbed ground. The surface height from the mud surface to the supporting rail was kept the same for all trials to ensure consistent flipper insertion depth.

To characterize the robot speed on different mud mixtures, two motion capture cameras (Optitrack, Prime 13W) were installed above the trackway to record the position of the robot in the world frame (x - fore-aft; y - lateral; z - vertical), at 120 frames per second (FPS). In addition, two video cameras (Logitech) were used to record experiment footage from both the side view and the top view at 30 FPS, to provide a close-up view of flipper-mud interaction, and flipper tracks in mud. In addition, the angular position and velocity of the motors were logged at a frequency of 380 Hz.

III. Results and Discussion

A. Robot speed exhibited non-monotonic dependence on mud water content: two distinct failure modes

The robot's average speed in the forward direction, v_x, exhibited a non-monotonic dependence on the mud water content, W (Fig. 2, blue markers). v_x was the largest at W = 25% (v_x = 6.5 $\pm$ 0.7 cm/s). For both $W > 25\%$ and $W < 25\%$, v_x decreased rapidly with only a few percent of water content variation: $v_x = 2.7 \pm 0.5$ cm/s at W = 24%; $v_x = 6.5 \pm 0.7$ cm/s at W = 25%; and v_x = 0.2 $\pm$ 0.07 cm/s at W = 32%. Interestingly, for both failing regions, the robot could often move forward relatively effectively during the first few steps (Fig. 2, green markers). However, tracking data indicated that the robot step length (*i.e.,* forward displacement during each cycle) decreased rapidly to close to 0 within the first 10 seconds for both high water content (Fig. 3I) and low water content (Fig. 3C).

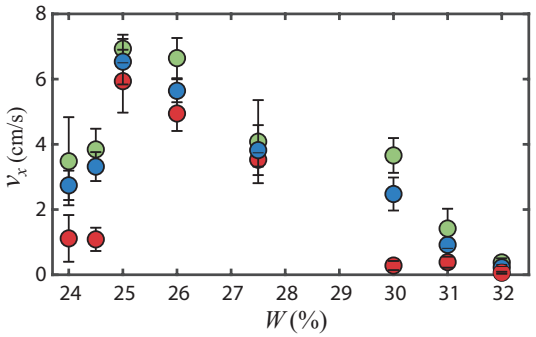

Fig. 2. Averaged robot forward speed versus mud water content. Blue, red, and green markers represent robot speed averaged from the entire trial, the last four steps, and the first four steps, respectively. Error bars represent the standard deviation of the averaged speed from three trials.

Examination of the flipper-mud interactions during the last few steps of robot locomotion at low water content (W = 24.5%) and high water content (W = 30%) suggested two distinct failure modes:

1. *Flipper entrapment at low water content.* Tracking data from W = 24.5% indicated a large periodic oscillation in the robot's forward displacement during the last few steps (Fig. 3B). Over the first half of the step (the flipper sweeping phase), the flipper slippage was small, and the robot could effectively advance forward. However, during the second half of the step (the flipper swing phase), it was observed that the flipper often failed to extract out of the mud surface fully, and instead dragged a large amount of material forward while entrapped underneath the mud surface (Fig. 3A). This flipper entrapment resulted in a large resistance force along the $-x$ direction, which inadvertently pushed the robot body backward and resulted in a negative displacement during the swing phase. The large forward displacement during the first half of the step and the significant negative displacement during the second half of the step contributed to the observed oscillation in the robot's forward position and the observed speed reduction on low water content mud.
2. *Large slippage at high water content.* Unlike the oscillatory robot fore-aft position observed from the low water content, tracking data from W = 30% showed that on high water content mud, the robot's fore-aft position remained constant throughout the entire step after the initial 8-9 steps (Fig. 3H). This indicated that the robot could not advance in the mud even during the flipper sweeping phase. It was observed that the robot flippers exhibited a large slippage during the sweeping phase and disturbing a large region of mud materials (Fig. 3G; Fig. 5C) as compared to locomotion on mud mixtures with lower water content (Fig. 3D; Fig. 5B), resulting in a reduced robot forward displacement over a step (Fig. 3I). In addition, it was observed that the distance between adjacent footprints decreased monotonically over time (Fig. 3G), eventually leading to a complete locomotion failure with zero advancement (Fig. 3H).

B. Force measurements revealed the failure mechanisms

We suspected that the large flipper slippage observed from mud mixtures with high water content was likely a result of reduced mud shear strength, whereas the flipper entrapment failure observed from low water content was likely a result of increased mud suction force in the vertical direction. To test our hypotheses and quantitatively understand the dependence of robot locomotion performance as a function of mud strength, we experimentally measured the mud reaction forces exerted on the robot flipper as it executed horizontal and vertical motion within mud mixtures with different water content.

1) Mud reaction force measurements: Two sets of experiments were performed: (i) a horizontal shear (Fig. 4A), where the flipper was dragged horizontally across the mud at a constant insertion depth of 3.5 cm, for a total shear distance of 10 cm; and (ii) a vertical extraction (Fig. 6A), where the flipper was pulled vertically from an initial insertion depth of 3.5 cm, the maximal insertion depth in the locomotion experiments. The extraction velocity was set to 0.5 m/s (corresponding to ω_β = 4.2 rad/s), the same as locomotion experiments. A high speed linear actuator (Heechoo) was used to actuate the flipper in both experiments. The shear resistive force, F_x,

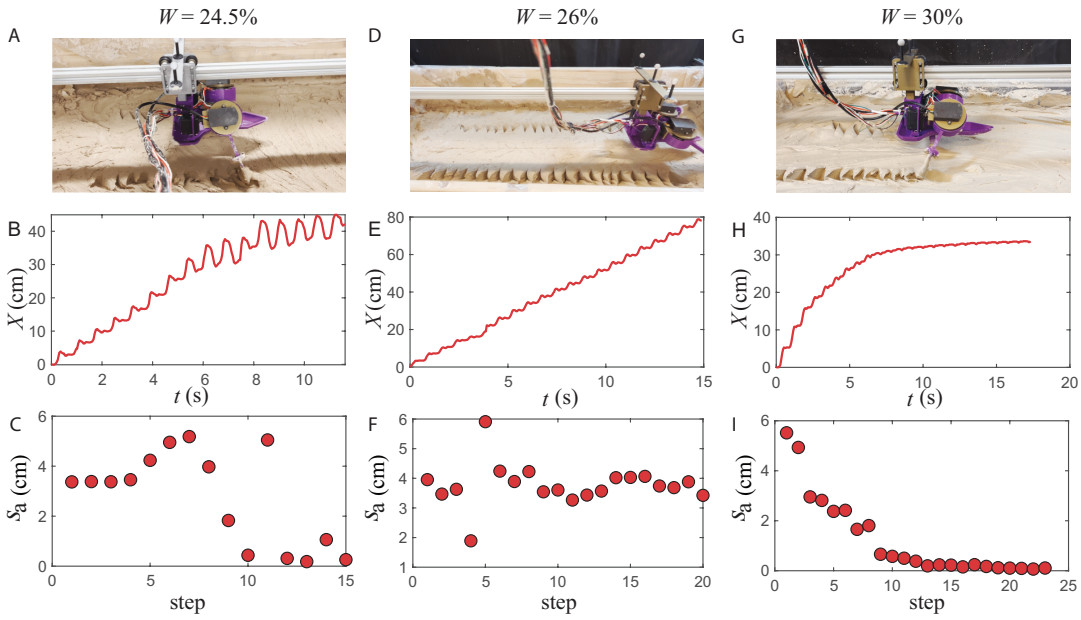

Fig. 3. Representative locomotion trials of the robot traversing mud mixtures with different water content (24.5%, 26%, and 30% shown in left, middle, and right columns, respectively). Experiment side-view, robot forward displacement versus time, and step length versus step number were shown in the top, middle, and bottom rows.

and the extraction resistive force, F_z, were measured using a force sensor (DYMH-103) mounted between the flipper and the linear actuator. For both shear and extraction experiments, three trials were performed at each mud water content.

2) Shear force measurements revealed the failure mechanism at high water content: We developed a highly simplified model to estimate the dependence of robot step length on mud shear strength. The model assumed that the flippers could propel the robot body forward without slipping in mud if the thrust force from both flippers, F_t (e.g., Fig. 4C, blue to yellow curves), was sufficient to overcome the required force, F_r (e.g., Fig. 4C, red horizontal line) due to drag and inertia.

The thrust force, F_t, was computed as the mud shear resistance force exerted on the flippers. The shear resistance force was assumed to increased linearly with the depth, the surface area of the intruder, and the shear strength of the material [30], [31]. For an infinitesimal segment of the flipper at a depth z, the shear resistance force was computed as $dF(\alpha) = l\cos(\alpha) \cdot kz \cdot dz$, where l is the flipper arm length, $l\cos(\alpha)dz$ represents the projected surface area of the flipper segment along the fore-aft direction, and k represents the mud shear strength coefficient that was empirically determined from the experimentally-measured average[1] shear force, $\bar{F}_a$ (Fig. 4B). Integrating dF from the mud surface to the insertion depth yields the thrust force for a given α.

The required force, F_r, was computed as the sum of the drag force exerted on the bottom of the robot, F_d, and the acceleration-related inertial force, F_i. The drag force, F_d, was modelled as the mud shear resistance force exerted on the bottom extrusion of the robot. F_i was the required force for the flippers to accelerate the robot body from stationary to the flipper speed, $l\omega_\alpha$, within a short duration, Δt. We estimated F_i as ma, where m is the robot mass and $a = \frac{l\omega_\alpha - 0}{\Delta t}$ is the magnitude of acceleration. Δt is the characteristic time constant insensitive to mud water content. In this study, we used $\Delta t = 0.054s$ for all trials.

When the thrust force from the flippers was sufficient to overcome the drag and inertial force (*i.e.,* $F_t(\alpha) > F_r$), the flippers were able to propel the body forward over "solidified" (*i.e.,* not yielding) mud, similar to the [11], [14] where the leg of a RHex robot stops sinking deeper once it generates sufficient supporting force from soft sand. We refer to this range of flipper angle, [-α_e, α_e], as the "effective advancing range". Once the effective advancing range was determined, the non-slip robot step length, S_a (Fig. 4D), could be computed as $S_a = 2l\sin(\alpha_e)$.

Experimental measurements revealed that as water content increased, the average mud shear force decreased monotonically (Fig. 4B). This led to a reduced F_t, and a significantly shortened effective advancing range. For example, as water content increased from 24% (Fig. 4C, top blue curve) to 30% (Fig. 4C, dark yellow curve), the effective advancing range reduced by more than 50% (Fig. 4C, solid red line), resulting in a large slippage and reduced robot forward step length, S_a (Fig. 4D). This decreased step length with increased water content successfully explained the locomotion failure observed at high water content.

The model predicted a constant step length for a given mud water content. However, in actual experiments, the robot step length at high water content was observed to begin at a larger step length, but quickly reduced to 0 cm after the initial few steps. We hypothesized that this was likely due to the feedback effect from the flipper encountering previously-disturbed material. Previous studies in dry granular media suggested

[1]For an intruder dragging in mud, the shear resistive force exerted on the intruder would first ramp up from zero at the onset of shear, then plateau to a steady-state shear force. The magnitude of the steady-state shear force represents the materials' mechanical strength [32], [33].

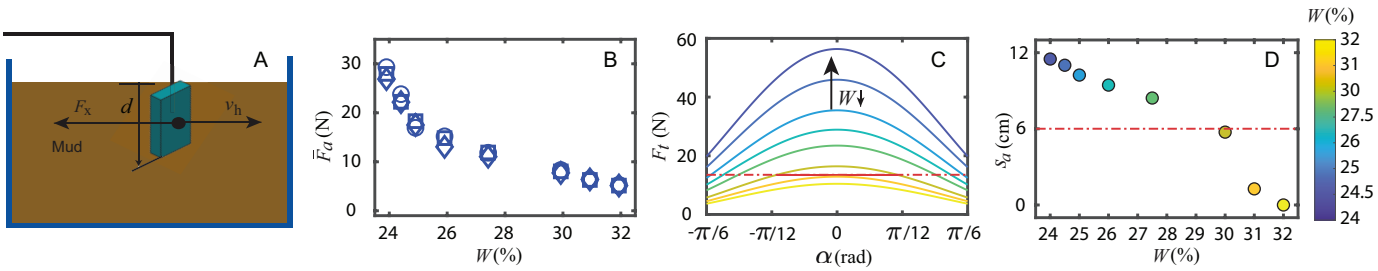

Fig. 4. Model-predicted mechanism behind the locomotion failure on high water content mud mixtures. (A) Experiment setup of shear force measurements. v_h indicates the moving direction of the flipper. F_x indicates the mud resistive force. (B) Experimentally measured averaged shear force on one flipper dragged through different water content. 3 trials were plotted for each water content. For each trial, the force signals from the last 4cm of the shear distance were averaged to obtain the steady-state shear force. (C) Model-predicted comparison between the thrust force and the required force in the fore-aft direction. Blue to yellow curves represent the model-estimated thrust force, F_t, during the sweeping phase, for water content from 24% to 32%, respectively, as shown in the color bar. The red horizontal line represents the required force, F_r, for a flipper sweeping speed of 4.2 rad/s. The solid range of the red line represents the "effective advancing range" for W = 30% (dark yellow). (D) Model predicted robot step length, S_a, computed from the effective advancing range. The red dashed line represents the minimum step length for the robot to generate sustainable forward motion without stepping into previously disturbed material.

that when a robot leg or flipper stepped into the proximity of previously-disturbed sand, the thrust force would decrease due to the reduced surface height [11], [13], [14]. Based on the robot kinematics, the minimal step length to avoid previously disturbed material, S_r, was 6 cm for our robot, below which the adjacent steps would begin to overlap (Fig. 5A). This minimal step length explained the decreasing robot step length observed at high water content (Fig. 3I): For $W \geq 30\%$, the model-predicted robot step length was below the minimal step length threshold (Fig. 4D, red dashed line). As a result, although the robot could initially advance forward, the subsequent step length would decrease as the flippers encounter previously-disturbed material. Experimentally-recorded robot footprints (Fig. 5C) corroborated with the model prediction, and confirmed that robot step length decreased rapidly once the footprints began to overlap, and eventually led to the observed locomotion failure.

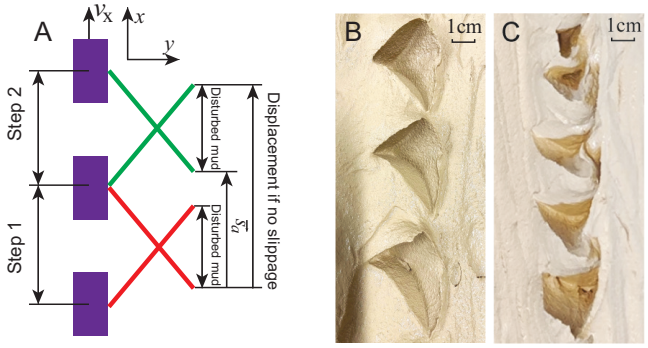

Fig. 5. Effect of disturbed mud on robot step length. (A) A top view diagram illustrating the minimal step length to prevent stepping into previously disturbed material. Purple rectangles represent the robot body at different steps. Red and green lines represent the starting and ending robot flipper positions from step 1 and 2, respectively. S_a represents the robot's step length. If S_a is smaller than half of the non-slip displacement length, the flipper at step 2 will encounter previously disturbed mud from step 1. (B) Robot flipper tracks from water content 28%, where the adjacent footprints did not overlap. (C) Robot flipper tracks from water content 30%, where the subsequent steps encountered previously disturbed material, resulting in a further reduced step length and the eventual failure.

3) Mud suction force measurements revealed the failure mechanism at low water content: The model explained the failure mechanism at high water content. However, it could not explain the reduced robot speed at low water content. If the flipper slippage was the primary cause of the observed locomotion failures, as water content decreased, the shear strength of the mud increased monotonically (Fig. 4B), which should result in a minimal slippage and increased robot speed at low water content (Fig. 4D). However, according to experiment measurements, robot speeds at W = 24% and 24.5% were less than 50% of that at W = 25%. This indicated that there must exist a different mechanism behind the observed failure at low water content.

To investigate the failure mechanism at low water content, we examined the mud resistive force during flipper extraction. Experimentally measured mud resistive force, F_z, rapidly increased to a maximum upon the initial flipper extraction motion (Fig. 6C). Then, once the flipper overcame this maximal suction force, F_z gradually decreased as the flipper insertion depth, d, reduced. Measurements also show that the maximal suction force, F_m, nearly doubled as water content W decreased by only 2%, from 26% to 24% (Fig. 6B).

We hypothesized that this significantly increased suction force impeded the flipper from fully extracting from the mud surface during the extraction phase. As a result, at the beginning of the swing phase, the flippers would be entrapped underneath the mud surface with a non-zero depth, d_e (Fig. 6C). As the entrapped flippers swing forward, they would propel the robot body backward during the swing phase, resulting in the observed step length reduction in low water content.

To test our hypothesis, we modelled the entrapment depth, d_e, and the resulting robot step length, as the water content decreased. The model assumed that the flipper could lift upward when the vertical mud resistive force, F_z (Fig. 6C, blue to red curves) was smaller than the maximal lifting force that the flipper could generate (Fig. 6C, red horizontal line). Once F_z reached the maximal force, the flipper would be entrapped at its current depth. The entrapment depth, d_e, could be determined from the intersection points between the F_z curves (Fig. 6C, blue to red curves) and the maximal lifting force (Fig. 6C, red horizontal line). Here the mud resistive force, F_z, was directly measured from the extraction force experiments,

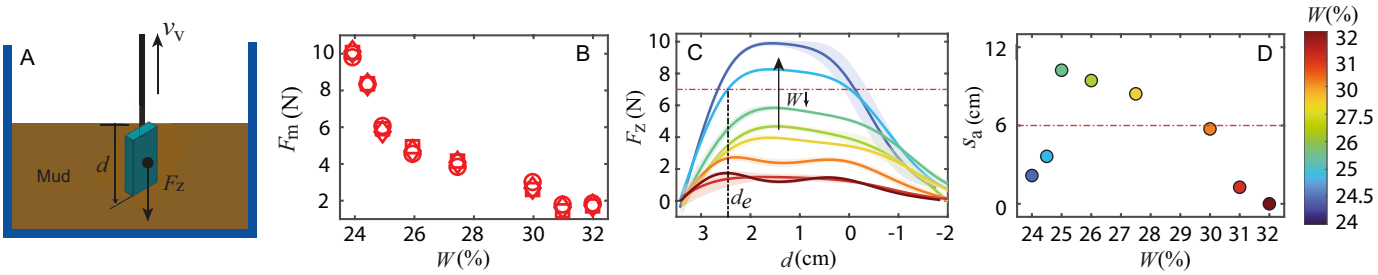

Fig. 6. Model-predicted mechanism behind the locomotion failure on low water content mud mixtures. (A) Experiment setup of extraction force measurements. v_v indicates the moving direction of the flipper. F_z indicates the mud resistive force during flipper extraction. (B) The maximum mud resistive force during flipper extraction, F_m, versus water content, W. 3 trials were plotted for each water content. (C) Comparison between the mud suction force on a flipper (blue to red curves), and the maximal force that a flipper could produce in the vertical direction (red dashed horizontal line). The entrapment depth, d_e, identified based on the intersection point between the cyan curve and the red horizontal line, was labeled for W = 24.5%. (D) The model-predicted step length due to both failure mechanisms, S_a, computed by subtracting the backward displacement during the flipper swing phase, S_b, from the forward displacement during the flipper sweeping phase, S_e.

whereas the maximal lifting force was estimated using the experimentally-measured maximal force that the flipper could produce before stalling, subtracting the gravitational force of the arm. A low pass filter was applied to F_z to facilitate the identification of the intersection point.

For mud mixtures with relatively large water content (Fig. 6C, red to green curves), the mud suction force was relatively small, and the flipper was able to fully extract to the mud surface (d_e = 0 cm) without exceeding the maximal lifting force. However, for mud mixtures with low water content (e.g., W = 24% and 24.5%, Fig. 6C, blue and cyan curves, respectively), the mud suction force was significantly larger, and the flipper would stall at d_e = 2.7 cm and 2.5 cm at the end of the extraction phase, respectively.

Based on the entrapment depth, we could compute the step length, S_a. The magnitude of $\overrightarrow{S_a}$ was computed by subtracting the magnitude of backward displacement during the swing phase, $\overrightarrow{S_b}$, from the forward displacement during the sweeping phase, $\overrightarrow{S_e}$. The magnitude of both $\overrightarrow{S_e}$ and $\overrightarrow{S_b}$ were computed using the same function form, $2l\sin(\alpha_e)$, as illustrated in Sec. III-B2. For S_e, the flipper insertion depth during sweeping phase, 3.5cm, was used to compute the shear resistance force and the resulting α_e; whereas for S_b, the entrapment depth, d_e, was used to compute the shear resistance force and the resulting α_e.

The increased entrapment depth explained the reduced robot performance observed at low water content. At W = 24.5%, the large flipper entrapment depth induced a large magnitude of negative displacement during the flipper swing phase, $|\overrightarrow{S_b}|$ = 7.4 cm. As a result, even the flipper slippage was small during the flipper sweeping phase, producing a forward displacement of $|\overrightarrow{S_e}|$ = 11 cm, the step length over the entire cycle, $\overrightarrow{S_e}+\overrightarrow{S_b}$, was significantly lower (3.6 cm, Fig. 6D blue marker). Despite the highly simplified model assumptions, the model-predicted dependence of robot step length on water content (Fig. 6D) successfully captured the non-monotonic trend of robot speed observed from experiments (Fig. 2).

In addition, a similar feedback effect of disturbed materials in Sec. III-B2 was observed at low water content, where the robot could advance forward over the first few steps, but the backward displacement increased over time and eventually

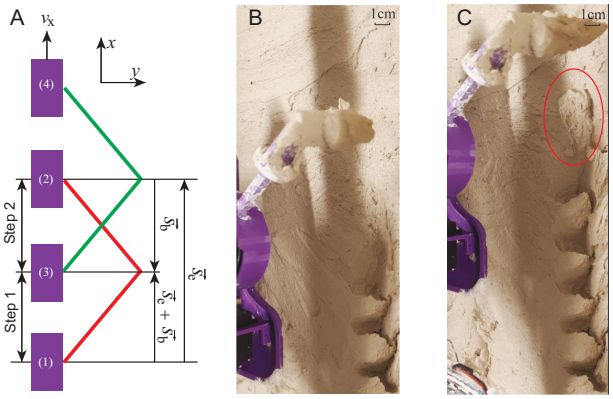

Fig. 7. Robot step length on mud mixture with low water content. (A) A top view diagram illustrating the actual step length, $\overrightarrow{S_a}$, computed as the sum of the forward displacement during the flipper sweeping phase, $\overrightarrow{S_e}$, and the backward displacement during the flipper swing phase,$\overrightarrow{S_b}$. Purple rectangles represent the robot body at different steps, with the number on the rectangle indicating the sequence: (1)→(2): step one, sweeping phase; (2)→(3): step one, swing phase; (3)→(4): step two, sweeping phase; (B) Robot flipper tracks from the initial few steps of water content 24.5%, where the mud dragged by the bottom of the flipper disturbed the mud surface as the flipper swung forward. (C) Robot flipper tracks from subsequent steps showing the increased disturbed range of mud surfaces, resulting in an increased surface height and actual insertion depth, leading to the observed flipper extraction failure.

led to failure (Fig. 3C). This is likely due to the increased extensional stress which amplified the surface disturbance. As shown in Fig. 6, the mud suction force did not decrease to 0 until approximately 2cm above the surface (Fig. 6), which is consistent with findings in previous research [34]. As a result, the mud adhered at the bottom of the flipper (Fig. 7B) would further increase the non-zero d_e, resulting in a larger entrapment depth at the subsequent steps (Fig. 7C) and led to the eventual failure.

IV. Adaptation of Locomotor Strategies to Mitigate Observed Failure Modes

In this section, we show that the simplified model could inform flipper strategy adaptations to mitigate the observed locomotion failures in mud. According to the model, the robot's step length was essentially governed by the comparison between the force a robot would generate from the mud, and

the force required for motion. As such, two groups of adaptation strategies could improve the locomotion performance: by adjusting the mud resistive force, or by adjusting the required force. Here we demonstrate the former for low water content mud, and the latter for high water content mud.

At high water content, by reducing the flipper sweeping speed, ω_α, the acceleration related inertial force, $F_i = \frac{ml\omega_\alpha}{\Delta t}$, could be reduced, resulting in a smaller required force, F_r (Fig. 8A, yellow to blue straight lines). The reduced required force would allow for a larger effective advancing range, thus producing a larger step length (Fig. 8B).This is similar to [11], where it was found that by lowering leg frequency, a legged robot could reach force balance in the vertical direction at a smaller leg penetration depth, to improve locomotion performance on loosely packed sand. Our model predicted that by reducing ω_α by less than 20% (from 4.2 rad/s to 3.3 rad/s), the robot step length, S_a, could increase above the critical threshold (Fig. 8B, red straight line) to mitigate the previously-observed slippage failure.

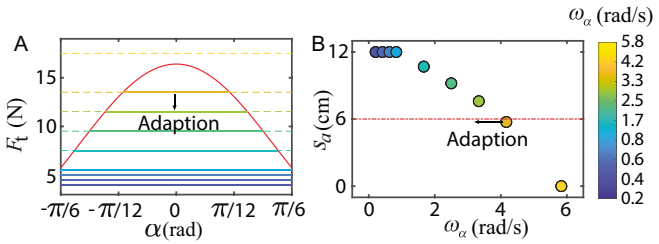

Fig. 8. Model predicted adaptation strategy for high water content. (A) The effect of flipper sweeping speed on the required force (blue to yellow horizontal lines). Color represents different sweeping angular velocities as shown in the color bar. The solid red curve represents the the flipper thrust force, F_t. The solid range of the horizontal lines represent the effective advancing range. (B) The effect of flipper sweeping velocity on robot step length. The markers represent the model-predicted step length. The red dashed line represents the minimal step length, below which the adjacent steps are expected to overlap and lead to robot locomotion failure.

At low water content, by reducing the flipper adduction speed, ω_β, the extraction resistive force was lowered (Fig. 9A, red to blue curves), and thus reducing the flipper entrapment depth (Fig. 9A, the depth where the curves intersected with the red horizontal line). The reduced entrapment depth would then allow the flipper to lift closer to or entirely out of the mud surface, reducing or eliminating the backward displacement during the flipper swing phase. Accordingly to the model prediction, by decreasing ω_β from 4.2 rad/s to 3.0 rad/s, the backward displacement could be reduced to 0 (Fig. 9B, red to blue markers), mitigating the previously-observed locomotion failure on low water content mud.

To validate the model-predicted adaptation strategies, we tested the robot locomotion with the model-suggested strategies on mud mixtures with W = 24.5% and W = 30%. Experimentally measured robot speed demonstrated a significant improvement for both mud mixtures (Fig. 10). For W = 30%, without the adaptation the robot speed was 2.5 cm/s (0.62 cm/s after the initial few steps). By decreasing ω_α from 4.2 rad/s to 3.3 rad/s, the robot speed increased by 224% (v_x = 8.1 cm/s). Similarly, for W = 24.5%, without the adaptation the robot speed was 3.5 cm/s (2.5 cm/s after the initial few steps).

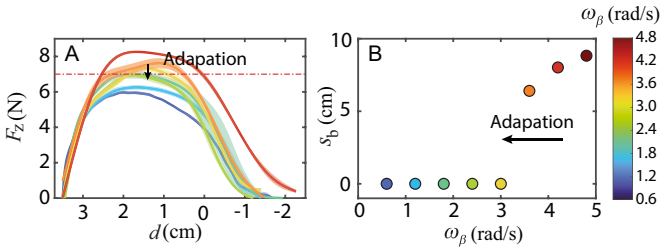

Fig. 9. Model predicted adaptation strategy for low water content. (A) The effect of flipper adduction speed on mud suction force. Colored curves represent the mud resistive force (mean and standard deviation) during flipper extraction from a depth of 3.5 cm with different speed. Red to blue represents ω_β from 4.8 to 0.6 rad/s, as indicated in the color bar. The horizontal red line represents the maximal lifting force that the flipper could produce. (B) The effect of flipper adduction velocity on the backward robot step length during the flipper swing phase.

By decreasing ω_β from 4.2 rad/s to 3.0 rad/s, the robot speed increased by 216% (v_x = 9.5 cm/s). The significantly improved robot performance demonstrated that a better understanding of the robot-substrate interactions could inform simple yet effective strategies for moving on complex terrains.

We note that while in this specific application scenario, the low-water-content failure could potentially be solved by alternative hardware variations (e.g., using a smaller flipper, a shorter arm, or a higher torque motor/gear), the dependence of the mud suction force and its effect on robot locomotion can be applied generally to guide robot design and control choices. For example, the model could guide the adaptation of flipper insertion depth and speed in natural nearshore environments where mud properties varies rapidly.

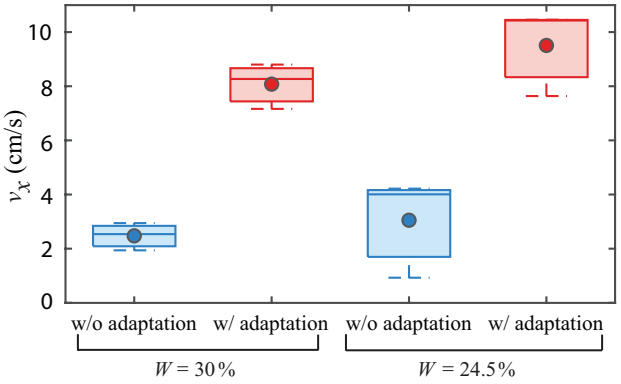

Fig. 10. Comparison of robot speed before (blue) and after (red) the model-suggested flipper speed adaptations on mud mixtures with high water content (W = 30%) and low water content (W = 24.5%).

V. CONCLUSION

In this study, we studied the locomotion of a flipper-driven robot on mud, and found that the robot's speed depended sensitively on both mud strength and flipper-mud interaction strategies. In mud mixtures with high water content, reduced mud shear strength could result in a large slippage as the robot flipper pushed the body forward, and cause the robot step length to decrease significantly within only a few steps. On the other hand, mud mixtures with low water content

posed a different challenge for terrestrial locomotion: the increased mud suction force could impede the flipper from full extraction, causing the robot body to oscillate in place and could not effectively advance forward. Understanding these underlying mechanisms behind the observed locomotion failure informed simple adjustments of flipper motion to mitigate. Locomotion experiments with model-suggested adaptation strategies demonstrated that a slight adjustment in flipper angular velocity during the mud interaction enabled a significant improvement (more than 200%) in robot speed for mud mixtures with both low and high water content. While this study is only a beginning step in developing general principles for terrestrial locomotion on mud, it demonstrated the potential for physics-based models to inform simple locomotion strategies and extend robot mobility beyond flat, rigid ground towards heterogeneous, deformable natural terrains. Future work could build upon the principles discovered in this study, to further explore effect of clay-to-sand ratio on robot locomotion performance, or integrate sensory feedback to enable autonomous adaptation of locomotion strategies in rapidly-varying natural muddy environments.

ACKNOWLEDGMENT

The authors would like to thank Jake Futterman for helping with the robot design; Sen Gao, Siyuan Meng, and Jiaze Tang for helping with preliminary data collection; Doug Jerolmack and Shravan Pradeep for helpful discussions.

REFERENCES

[1] J. Y. Wong, *Terramechanics and off-road vehicle engineering: terrain behaviour, off-road vehicle performance and design*. Butterworth-heinemann, 2009.

[2] S. Godon, A. Ristolainen, and M. Kruusmaa, "An insight on mud behavior upon stepping," *IEEE Robotics and Automation Letters*, vol. 7, no. 4, pp. 11 039–11 046, 2022.

[3] S. Zhang, Y. Zhou, M. Xu, X. Liang, J. Liu, and J. Yang, "Amphihex-i: Locomotory performance in amphibious environments with specially designed transformable flipper legs," *IEEE/ASME Transactions on Mechatronics*, vol. 21, no. 3, pp. 1720–1731, 2016.

[4] S. Choi, G. Ji, J. Park, H. Kim, J. Mun, J. H. Lee, and J. Hwangbo, "Learning quadrupedal locomotion on deformable terrain," *Science Robotics*, vol. 8, no. 74, p. eade2256, 2023.

[5] P. Coussot and J. M. Piau, "On the behavior of fine mud suspensions," *Rheologica acta*, vol. 33, no. 3, pp. 175–184, 1994.

[6] P. Coussot, "Structural similarity and transition from newtonian to non-newtonian behavior for clay-water suspensions," *Physical review letters*, vol. 74, no. 20, p. 3971, 1995.

[7] R. Kostynick, H. Matinpour, S. Pradeep, S. Haber, A. Sauret, E. Meiburg, T. Dunne, P. Arratia, and D. Jerolmack, "Rheology of debris flow materials is controlled by the distance from jamming," *Proceedings of the National Academy of Sciences*, vol. 119, no. 44, p. e2209109119, 2022.

[8] M. H. Raibert, *Legged robots that balance*. MIT press, 1986.

[9] U. Saranli, M. Buehler, and D. E. Koditschek, "Rhex: A simple and highly mobile hexapod robot," *The International Journal of Robotics Research*, vol. 20, no. 7, pp. 616–631, 2001.

[10] S. Kim, J. E. Clark, and M. R. Cutkosky, "isprawl: Design and tuning for high-speed autonomous open-loop running," *The International Journal of Robotics Research*, vol. 25, no. 9, pp. 903–912, 2006.

[11] C. Li, P. B. Umbanhowar, H. Komsuoglu, D. E. Koditschek, and D. I. Goldman, "Sensitive dependence of the motion of a legged robot on granular media," *Proceedings of the National Academy of Sciences*, vol. 106, no. 9, pp. 3029–3034, 2009.

[12] F. Qian, T. Zhang, C. Li, P. Masarati, A. M. Hoover, P. Birkmeyer, A. Pullin, R. S. Fearing, and D. I. Goldman, "Walking and running on yielding and fluidizing ground," *Robotics: Science and Systems*, p. 345, 2013.

[13] N. Mazouchova, P. B. Umbanhowar, and D. I. Goldman, "Flipper-driven terrestrial locomotion of a sea turtle-inspired robot," *Bioinspiration & biomimetics*, vol. 8, no. 2, p. 026007, 2013.

[14] F. Qian, T. Zhang, W. Korff, P. B. Umbanhowar, R. J. Full, and D. I. Goldman, "Principles of appendage design in robots and animals determining terradynamic performance on flowable ground," *Bioinspiration & biomimetics*, vol. 10, no. 5, p. 056014, 2015.

[15] B. McInroe, H. C. Astley, C. Gong, S. M. Kawano, P. E. Schiebel, J. M. Rieser, H. Choset, R. W. Blob, and D. I. Goldman, "Tail use improves performance on soft substrates in models of early vertebrate land locomotors," *Science*, vol. 353, no. 6295, pp. 154–158, 2016.

[16] D. Bonn, M. M. Denn, L. Berthier, T. Divoux, and S. Manneville, "Yield stress materials in soft condensed matter," *Reviews of Modern Physics*, vol. 89, no. 3, p. 035005, 2017.

[17] R. M. Nedderman *et al.*, *Statics and kinematics of granular materials*. Cambridge University Press Cambridge, 1992, vol. 352.

[18] H. M. Jaeger and S. R. Nagel, "Physics of the granular state," *Science*, vol. 255, no. 5051, pp. 1523–1531, 1992.

[19] H. Bagheri, V. Jayanetti, H. R. Burch, C. E. Brenner, B. R. Bethke, and H. Marvi, "Mechanics of bipedal and quadrupedal locomotion on dry and wet granular media," *Journal of Field Robotics*, vol. 40, no. 2, pp. 161–172, 2023.

[20] M. Caggioni, V. Trappe, and P. T. Spicer, "Variations of the herschel–bulkley exponent reflecting contributions of the viscous continuous phase to the shear rate-dependent stress of soft glassy materials," *Journal of Rheology*, vol. 64, no. 2, pp. 413–422, 2020.

[21] A. Shakeel, A. Kirichek, and C. Chassagne, "Rheological analysis of mud from port of hamburg, germany," *Journal of Soils and Sediments*, pp. 1–10, 2019.

[22] S. Nie, Q. Jiang, L. Cui, and C. Zhang, "Investigation on solid-liquid transition of soft mud under steady and oscillatory shear loads," *Sedimentary Geology*, vol. 397, p. 105570, 2020.

[23] S. M. Contreras and T. R. Davies, "Coarse-grained debris-flows: hysteresis and time-dependent rheology," *Journal of Hydraulic Engineering*, vol. 126, no. 12, pp. 938–941, 2000.

[24] D. J. Hodgson, M. Hermes, E. Blanco, and W. C. Poon, "Granulation and suspension rheology: A unified treatment," *Journal of Rheology*, vol. 66, no. 5, pp. 853–858, 2022.

[25] X. Liang, M. Xu, L. Xu, P. Liu, X. Ren, Z. Kong, J. Yang, and S. Zhang, "The amphihex: A novel amphibious robot with transformable leg-flipper composite propulsion mechanism," in *2012 IEEE/RSJ International Conference on Intelligent Robots and Systems*. IEEE, 2012, pp. 3667–3672.

[26] S. Zhang, Y. Zhou, M. Xu, X. Liang, J. Liu, and J. Yang, "Amphihex-i: Locomotory performance in amphibious environments with specially designed transformable flipper legs," *IEEE/ASME Transactions on Mechatronics*, vol. 21, no. 3, pp. 1720–1731, 2016.

[27] S. Godon, M. Kruusmaa, and A. Ristolainen, "Maneuvering on non-newtonian fluidic terrain: a survey of animal and bio-inspired robot locomotion techniques on soft yielding grounds," *Frontiers in Robotics and AI*, vol. 10, p. 1113881, 2023.

[28] J. Aguilar, T. Zhang, F. Qian, M. Kingsbury, B. McInroe, N. Mazouchova, C. Li, R. Maladen, C. Gong, M. Travers *et al.*, "A review on locomotion robophysics: the study of movement at the intersection of robotics, soft matter and dynamical systems," *Reports on Progress in Physics*, vol. 79, no. 11, p. 110001, 2016.

[29] S. M. Kawano and R. W. Blob, "Propulsive forces of mudskipper fins and salamander limbs during terrestrial locomotion: implications for the invasion of land," *Integrative and comparative biology*, vol. 53, no. 2, pp. 283–294, 2013.

[30] R. Albert, M. Pfeifer, A.-L. Barabási, and P. Schiffer, "Slow drag in a granular medium," *Physical review letters*, vol. 82, no. 1, p. 205, 1999.

[31] C. Li, T. Zhang, and D. I. Goldman, "A terradynamics of legged locomotion on granular media," *science*, vol. 339, no. 6126, pp. 1408–1412, 2013.

[32] N. Gravish, P. B. Umbanhowar, and D. I. Goldman, "Force and flow at the onset of drag in plowed granular media," *Physical Review E*, vol. 89, no. 4, p. 042202, 2014.

[33] F. Qian, D. Lee, G. Nikolich, D. Koditschek, and D. Jerolmack, "Rapid in situ characterization of soil erodibility with a field deployable robot," *Journal of Geophysical Research: Earth Surface*, vol. 124, no. 5, pp. 1261–1280, 2019.

[34] S. Godon, A. Ristolainen, and M. Kruusmaa, "An insight on mud behavior upon stepping," *IEEE Robotics and Automation Letters*, vol. 7, no. 4, pp. 11 039–11 046, 2022.